รายงานฉบับสมบูรณ์

โครงการ Molecular Structure and Assembly of *Bacillus thuringiensis* Toxin-Induced Pores in Lipid Membranes

การศึกษาโครงสร้างและการก่อตัวของรูรั่วในผนังไขมันโดยโปรตีนสารพิษจากแบคทีเรีย *Bacillus thuringiensis*

โดย นายชนันท์ อังศุธนสมบัติ

31 พฤษภาคม 2556

สัญญาเลขที่ ***BRG53-8-0007***

รายงานฉบับสมบูรณ์

โครงการ Molecular Structure and Assembly of *Bacillus thuringiensis* Toxin-Induced Pores in Lipid Membranes

การศึกษาโครงสร้างและการก่อตัวของรูรั่วในผนังไขมันโดยโปรตีนสารพิษจากแบคทีเรีย *Bacillus thuringiensis*

ผู้วิจัย
นายชนันท์ อังศุธนสมบัติ

สังกัด
สถาบันชีววิทยาศาสตร์โมเลกุล
มหาวิทยาลัยมหิดล

สนับสนุนโดยสำนักงานกองทุนสนับสนุนการวิจัย

Acknowledgements

I am grateful to Drs. Gerd Katzenmeier, Somphob Leetachewa and Chalermpol Karnchanawarin for valuable comments and helpful discussion and to Somsri Sakdee and Anchalee Nirachanon for technical assistance. This work was supported in part by grant number BRG53-8-0007 from the Thailand Research Fund. Golden Jubilee Ph.D. research scholarships to Drs. Thanate Juntadech (RGJ-10) and Anon Thammasittirong (RGJ-10) are gratefully acknowledged.

Chanan Angsuthanasombat

June 30, 2013

Project Code: BRG53-8-0007

Project Title:

Molecular Structure and Assembly of *Bacillus thuringiensis* Toxin-Induced Pores in Lipid Membranes

การศึกษาโครงสร้างและการก่อตัวของรูรั่วในผนังไขมันโดยโปรตีนสารพิษจากแบคทีเรีย *Bacillus thuringiensis*

Investigator: Chanan Angsuthanasombat, Ph.D.

Laboratory of Molecular Biophysics and Structural Biochemistry
Institute of Molecular Biosciences, Mahidol University

E-mail: chanan.ang@mahidol.ac.th

Project Period: 3 years (June 1, 2010 - May 31, 2013)

Abstract

Cry4Aa and Cry4Ba δ-endotoxins produced from *Bacillus thuringiensis* are specifically toxic to mosquito-larvae by forming ion-permeable pores in the midgut cell membrane. One proposed toxic mechanism *via* an "umbrella-like" model involves membrane penetration and pore formation of the α4-loop-α5 hairpin. In this report, functional importance of the Cry4Aa α4-α5 loop structure, especially the Pro-rich sequence ($Pro^{193}Pro^{194}\_Pro^{196}$) was examined. Val-substitutions (P193V, P194V and P196V) were found to reduce toxicity against *Aedes aegypti* mosquito-larvae. In addition, enhancing the flexibility of the α4-α5 loop through P193G, P194G and P196G mutations adversely affected the larvicidal activity, suggesting that loop rigidity resulted from the unique cyclic structure of Pro is important for toxicity. Structural analysis of Pro^{193} showed that this most critical residue is in close contact with the surrounding residues, thus playing an additional role in maintaining tertiary structure of the toxin. MD simulations of the 65-kDa Cry4Aa structure in solution revealed that the α4-α5 loop is substantially stable, suggesting that an important implication in toxin activity of the Cry4Aa α4-α5 loop structure. Structurally stable-Cry4Ba mutant toxins of both larvicidal-active (N166D) and inactive (N166A and N166I) were also characterized for their relative activities in liposomal-membrane permeation and single-channel formation. Similar to the wild type, the N166D bio-active mutant was still capable of releasing entrapped calcein from lipid vesicles. Conversely, the two other bio-inactive mutants showed a dramatic decrease in causing membrane permeation. When the N166D mutant was incorporated into planar lipid bilayers, it produced single-channel currents with a maximum conductance of ~425 pS comparable to the wild type. However, maximum conductances for single K^+-channels formed by both bio-inactive mutants were reduced to approximately 165-205 pS. Structural dynamics of 60-ns simulations of a trimeric α4-α5 pore model in a fully hydrated-DMPC system revealed that an open-pore structure could be observed only for the simulated pores of the wild type and N166D. The number of lipid molecules surrounding both wild-type and N166D pores are relatively higher than those of N166A and N166I pores. Altogether, our results signify that the polarity at the α4-α5 loop residue–Asn^{166} is directly involved in ion permeation through the Cry4Ba toxin-induced pore and pore opening at the membrane-water interface.

Keywords **:** Ion channel; MD simulations; Larvicidal activity; Loop rigidity; Polarity; Pro-rich sequence; Mutagenesis; Trimeric pore structure

1. Introduction

Cry insecticidal proteins known as δ-endotoxins are produced in the form of crystalline inclusions during sporulation by the Gram-positive soil bacterium *Bacillus thuringiensis* (*Bt*). These crystal toxins are cytolytic pore-forming toxins that are lethal to various insect larvae [Schnepf *et al*., 1998]. For example, Cry4Aa and Cry4Ba, two closely related δ-endotoxins made by *Bt* subsp. *israelensis* (*Bti*), are highly toxic to the larvae of *Aedes* and *Anopheles* mosquitoes, vectors of dengue viruses and malaria, respectively [Angsuthanasombat, 2010; Federici *et al*., 2010]. Biochemically, the Cry inclusions are solubilized in the midgut lumen of susceptible insect larvae at alkaline pH for both dipterans and lepidopterans, and proteolytically activated by gut proteases to yield the active toxins of ~65-kDa. Subsequently, the activated toxins bind specifically to a variety of receptors such as GPI (glycosylphosphatidylinositol)-anchored aminopeptidase-N and GPI-anchored alkaline phosphatase that are found on the brush-border membrane (BBM) of midgut epithelial cells [Pigott & Ellar, 2007; Pardo-López *et al*., 2013]. This toxin-receptor interaction could assist toxin penetration into the cell membrane, leading to the formation of ion-permeable pores that eventually cause osmotic lysis of the target cells. Although our understanding of toxic mechanisms of *Bt*-Cry toxins has expanded dramatically over the last decade [Schnepf *et al*., 1998; Angsuthanasombat, 2010; Pardo-López *et al*., 2013], their exact mechanisms of action at the molecular level still remain to be explored.

We now know the crystal structures of a number of the *Bt*-Cry toxins [Boonserm *et al*., 2005; 2006; Li *et al*., 1991; Morse *et al*., 2001; Grochulski *et al*., 1995], including the two closely related *Bti*-mosquito-active toxins, Cry4aa and Cry4Ba. Despite their broad diversity in insecticidal spectra, all the known Cry structures of the 65-kDa activated form reveal a high degree of overall structural conservation, suggesting that they all employ a common mode of action. The structures display a three-distinct domain construction (an α-helical bundle, a three-β-sheet assembly and a β-sandwich) which resembles a wedge-shaped body with size of about 55×65×75 Å [Angsuthanasombat, 2010; Li *et al*., 1991]. Of particular interest, it is structurally obvious that the helical domain is likely to be a transmembrane pore-forming unit, given that at least five helices, *i.e.* α3, α4, α5, α6 and α7, are of sufficient length (>30Å) to span the lipid membrane [Angsuthanasombat, 2010; Li *et al*., 1991]. Additionally, this helical domain has been experimentally proven capable of membrane-inserted pore formation, albeit in the absence of specific receptors [Grochulski *et al*., 1995; Slatin *et al*., 1990; Peyronnet *et al*., 2001; 2002].

Nonetheless, the precise structural feature of such a Cry toxin-induced pore is not yet known. At present, it seems that the so-called “umbrella-like” model is still the most well-known description for depicting the membrane-insertion and pore-formation stages of the three-domain Cry toxins [Knowles, 1994; Gazit *et al*., 1998]. This proposed model entails an insertion of the two pore-lining helices, *i.e.* α4 and α5, into the lipid membrane as a helical hairpin arrangement, and in so doing the remaining helices spread over the membrane surface like the opening of an

umbrella [Gazit *et al*., 1998]. Substantial evidence has preferentially supported this mechanistic model by signifying the role of both α4 and α5 in the toxicity of different Cry toxins. For instance, numerous studies of Cry toxin-induced pore formation suggested that α4 lines the pore lumen and plays a part in ion conduction [Masson *et al*., 1999; Sramala *et al*., 2001], while α5 which is rather hydrophobic and could take part in toxin-pore oligomerization [Nunez-Valdez *et al*., 2001; Likitvivatanavong *et al*., 2006].

In our earlier study, we provided direct evidence for liposomal membrane-permeating activity of the α4-loop-α5 fragment purified from the engineered Cry4Ba toxin [Leetachewa *et al*., 2006]. Similar studies by other workers *via* the use of synthetic peptides corresponding to α4, α5 and α4-loop-α5 of Cry1Ac clearly demonstrated that the loop linking α4 and α5 is basically required for efficient penetration of these two transmembrane helices into the lipid bilayers to induce membrane permeabilization [Gerber & Shai, 2000]. This notion was supported by our results that revealed a structural requirement for larvicidal activity of one highly conserved aromatic residue found within the α4-α5 loop of both Cry4Aa (Tyr^{202}) and Cry4Ba (Tyr^{170}), conceivably for stabilizing the membrane-associated pore complex [Kanintronkul *et al*., 2003; Pornwiroon *et al*., 2004]. Other workers showed that one Cry1Aa mutant, Y153D, in which the conserved aromatic residue–Tyr^{153} in the α4-α5 loop region (corresponding to Cry4Aa-Tyr^{202} or Cry4Ba-Tyr^{170}), exhibited a loss in larvicidal activity due to its inability to incorporate into BBM vesicles [Chen *et al*., 1995]. Likewise, two other conserved aromatic residues (*i.e.* Tyr^{249} and Phe^{264}), which are oriented on the same side of Cry4Ba-α7, were also found to be important for larvicidal activity activity [Tiewsiri & Angsuthanasombat, 2007]. The conserved helix 7 may undergo a conformational change to convert into a membrane-inserted β-hairpin which acts as a lipid anchor needed for membrane penetration by the pore-forming α4-loop-α5 [Tiewsiri *et al*., 2009].

2. Experimental Procedures

2.1. Construction of Toxin Mutants

The recombinant plasmid pMEx-B4A encoding the 130-kDa Cry4Aa toxin under control of the *tac* promoter together with the *cry4Ba* promoter [Boonserm *et al*., 2004] was used as a template for the introduction of single mutations. Fourteen pairs of complementary mutagenic primers (**Table 1**) designed according to the *cry4Aa* gene sequence were purchased from Sigma Proligo (Singapore). All mutant plasmids were generated by polymerase chain reaction using high-fidelity Phusion DNA polymerase (Finnzymes), following the procedure of the QuickChange™ Mutagenesis Kit (Stratagene). Selected clones with the mutations were first identified by restriction digestion of the plasmids and then verified by DNA sequencing.

2.2. Toxin Expression, Solubilization, Activation & Purification

Cry4Aa, Cry4Ba wild-type and their mutant toxins were over-expressed in *Escherichia coli* JM109 upon induction with isopropyl-β-D-thiogalactopyranoside (0.1 mM final concentration) as described previously. Toxin inclusions (1-2 mg/ml), which were centrifugally purified from French Press-disrupted lysates, were solubilized by incubation at 37 °C for 1 h in carbonate

buffer (50 mM Na_2CO_3/$NaHCO_3$, pH 9.0). Solubilized protoxins were then activated with trypsin (tolylsulfonyl phenylalanyl chloromethyl ketone-treated; Sigma) at a ratio of 1:20 enzyme/toxin (w/w) at 37 °C for 16 h. After SDS-PAGE (sodium dodecyl sulfate-polyacrylamide gel electrophoresis) analysis, the trypsin-treated fraction was concentrated by ultrafiltration (30-kDa cutoff) and further purified by a size-exclusion FPLC system (Superose 12™ column; GE Healthcare Life Biosciences) eluted with the carbonate buffer (pH 9.0) as described elsewhere [Tiewsiri & Angsuthanasombat, 2007]. Protein concentrations were determined using the Bradford-based protein microassay (Bio-Rad), with BSA as a standard protein.

2.3. Larvicidal Activity Assays

Bioassays for mosquito-larvicidal activity were done at room temperature (~25 °C) for 24 h using 2 day-old *A. aegypti* larvae as described previously [Sramala *et al*., 2001]. The assays were carried out in a 48-well polystyrene plate (11.3-mm well diameter) with 1 ml/well of toxin inclusion suspension (5 μg/ml suspended in distilled water). 100 larvae (10 larvae/well × 10 wells) were used for treatment with each toxin sample.

2.4. Circular Dichroism (CD) Measurements

CD spectra of the purified trypsin-treated toxins were measured with a Jasco J-715 spectropolarimeter (calibrated with a solution of camphorsulfonic acid), scanned in the far UV region (185-280 nm) at 25 °C using a rectangular quartz cuvette (0.2-mm path length) as described previously [Tiewsiri & Angsuthanasombat, 2007]. Protein samples were prepared in sodium phosphate buffer (50 mM NaH_2PO_4/ Na_2HPO_4, pH 9.0), with concentrations of 0.30-0.50 mg/ml, as determined by far UV absorbance. CD measurements were recorded at a rate of 50 nm/min with a spectral bandwidth of 2 nm. CD signals (mdeg), which were averaged from at least five accumulations and then corrected for solvent baseline, were finally converted to mean residue ellipticity ([θ], deg.cm^2/dmole).

2.5. Intrinsic Fluorescence Measurements

The intrinsic fluorescence spectra were obtained by emission scanning of the FPLC-purified trypsin-activated toxins using Jasco FP-6300 spectrofluorometer. The protein samples were excited at 280 nm and the emission wavelengths were observed from 300 to 500 nm. Excitation and emission slit widths are 5 and 2.5 nm, respectively.

2.6. Lipid Vesicle Preparation & Fluorescence Dye-Leakage Assays

Large unilamellar vesicles (LUVs, mean diameter of ~100 nm) encapsulated with calcein at a self-quenching concentration of 60 mM in 50 mM Na_2CO_3/$NaHCO_3$, pH 9.0, were prepared from a lipid mixture (Avanti Polar Lipid) of phosphatidylcholine (PC), phosphatidylethanolamine (PE), cholesterol (Ch) (10:10:1, w/w) by the extrusion method according to standard procedures described previously [Leetachewa *et al*., 2006]. Suspension concentrations of calcein-loaded LUVs (in 150 mM NaCl, 50 mM Na_2CO_3/$NaHCO_3$, pH 9.0) were estimated by measuring the lipid phosphorus content, and a final concentration of 2.5 μM was used for calcein leakage assays.

Release of entrapped calcein was monitored as function of time *t* by measuring an increase in fluorescence emission at 520 nm (excitation 495 nm) on a LS50 spectrofluorometer (Perkin–Elmer) at 25 ºC. Efflux curves were normalized to percentage of release activity or fluorescence recovery F_t which is defined as $F_t = (I_t - I_0)/(I_{max} - I_0) \times 100$, where I_0 is initial fluorescence intensity, I_{max} is the total fluorescence intensity observed upon addition of Triton X-100 (causing

100% calcein leakage) and I_t is the fluorescence intensity observed after adding the tested toxins at time *t*. For the concentration-activity profile, the plot of fractional release activity *Y* (P_{TL} /1 − P_{TL}) versus toxin concentration [T] was fitted to the Hill equation, P_{TL} / 1 − P_{TL} = $[T]^n$ / EC_{50}, where P_{TL} is the probability of finding toxin-liposome complex T_nL to give the Hill coefficient *n* and the effective concentration EC_{50}.

2.7. Planar Lipid Bilayers (PLBs) & Single Channel Analysis

PLBs were formed at 25 ºC by painting a 7:2:1 (w/w) lipid mixture of PE, PC, and Ch on a 200-μm aperture in a 1ml-Delrin cup, with membrane capacitance values of 200-250 pF as described earlier [Puntheeranurak *et al*., 2004]. Toxin incorporation was facilitated by stirring the protein-containing buffer (150 mM KCl, 10 mM Tris-HCl, pH 8.5) in the *cis* chamber along with applying a 100-mV holding potential across the lipid bilayer. Single-channel currents were recorded with an Axopatch-1D amplifier. Signals, which were low-pass filtered at 600 Hz, were digitized with a Digidata 1200 analogue-to-digital converter using Axoscope 8.0 software at a 50-kHz sampling frequency. Channel conductances were determined from the slope of current-voltage (I-V) relations plotted between the observed current steps and the corresponding applied voltage.

2.8. Pore Modeling & Molecular Dynamics (MD) Simulations

3D model of a trimeric pore consisting of α4-loop-α5 hairpins of Cry4Ba extracted from the X-ray trimer structure (PDB ID 1W99) [Boonserm *et al*., 2005] was initially constructed *via* protein docking between the two helices, α4 and α5, using Hex program. The pore model was inserted into a DMPC (1,2 dimyristoyl-*sn*-glycero-3-phosphocholine) bilayer constructed by using membrane builder module from CHARMM GUI server. Two water layers and sodium and chloride ions were added to the DMPC bilayer model using VMD program. The final pore model in water/lipid system consisted of three α4-α5 hairpins (34,575 atoms) in a bilayer of 114 DMPC lipids, 5991 water molecules, 15 Na^+ ions and 18 Cl^- ions. The system was energy minimized for 10,000 steps, then heated from temperature 0 to 300 K for 100 ps, equilibrated at pressure 1 atm for 5 ns and then ran as the final production for 60 ns using NAMD program running on a computer with 8 CPUs at 1 ns/day.

The equilibrated coordinates of the 5-ns wild-type pore system were used as a template for MD simulations of the mutant systems. Asp, Ala and Ile were substituted respectively for Asn^{166} in the pore model using VMD program. Three more sodium ions were added to N166D pore model to neutralize the system. The three pore models of Cry4Ba mutants were energy minimized for 1000 steps, then heated to 300 K for 20 ps, equilibrated at 1 atm for 10 ps, and finally ran as unrestrained molecular dynamics simulations for 60 ns. Analyses of MD trajectories were done *via* VMD program.

For *MD simulations of the Cry4Aa structure in KCl solution,* the structural model [Boonserm *et al*., 2006] of the Cry4Aa monomer in 150 mM KCl solution box was used as the initial system for 10-ns simulations. MD simulations were performed using NAMD 2.6 program and CHARMM27 force field. The system was energy minimized and then equilibrated for 50 ps at temperature of 298 K and pressure of 1 atm with all heavy atoms of the protein under harmonic constraints (a force constant of 2 kcal/mol/$Å^2$). Subsequently, without constraints, 10-ns simulations were performed at the same conditions as those used for equilibration. All the other parameters used in the simulations were explained elsewhere [Taveecharoenkool *et al*., 2010].

3. Results & Discussion

3.1. Structural Importance of the Cry4Aa α4-α5 Loop

3.1.1. Hydrophobic Feature of the Cry4Aa Pro-Rich Sequence

It is hypothesized that the previously shown importance of the Cry4Aa Pro-rich region ($Pro^{193}Pro^{194}$_Pro^{196}) within the α4-α5 loop composing the pore-forming domain (**Fig. 1**) for larvicidal activity [Tapaneeyakorn *et al*., 2005] could be due to its hydrophobic feature. To test this notion, the three Pro residues were replaced separately with Val, a hydrophobic residue with molecular mass similar to Pro. When each mutant toxin was expressed in *E. coli* cells, all were produced as inclusions at levels comparable to the wild type (**Fig. 2**). Assessment of alkaline solubility of the mutant toxins revealed that toxin inclusions of P194V and P196V were totally soluble (**Fig. 3A**). However, a nearly complete loss of the inclusion solubility was observed for the P193V mutant, implying that substitution at Cry4Aa-Pro^{193} could disturb the structural characteristic of the toxin and hence cause the formation of insoluble aggregates.

When *E. coli* cells expressing each Val-substituted mutant toxin were tested for their biological activity against *A. aegypti* mosquito-larvae, it was found that all Pro-to-Val mutants displayed a significant decrease in larvicidal activity (**Fig. 4**), indicating that Val cannot compensate the three Pro residues. Side-chain structures of these two hydrophobic amino acids are obviously different, *i.e.*, Pro has a hydrophobic plate while Val has a hydrophobic alkyl chain, suggesting an importance of the specific structure rather than hydrophobicity *per se* for function of the critical Pro residues.

3.1.2. Structural Essential of the Pro-Rich Sequence for Cry4Aa Activity

Generally, the backbone adjacent to Pro is conformationally rigid since the unique cyclic structure of the Pro's side-chain locks the backbone dihedral angle. Thus, the three Pro residues (Pro^{193}, Pro^{194} and Pro^{196}) would make the loop linking α4 and α5 of the Cry4Aa toxin to be highly rigid. To determine whether loop rigidity provided by the Pro-rich sequence is relevant to biological activity of the Cry4Aa toxin, the three Pro residues (Pro^{193}, Pro^{194} and Pro^{196}) were substituted with Gly, the most flexible amino acid residue. It was found that the resulting Gly-substituted mutants were produced in *E. coli* cells as inclusion bodies at levels similar to that of the wild-type toxin (**Fig. 2**).

Bioassays of these mutant toxins revealed that P194G and P196G mutations reduced larvicidal activity of approximately 20-30% and P193G mutation resulted in a 50% loss in toxicity (**Fig. 4**). Compared to previously constructed α4-α5 loop mutant, P193A, which exhibited a 30% decrease in toxicity [Tapaneeyakorn *et al*., 2005], Gly-substitutions which introduce more flexibility to the loop had higher adverse effect on larvicidal activity. It was shown that Pro^{345} located near the turn between transmembrane α8 and α9 is important for membrane

insertion of the diphtheria toxin as it may determine the conformation of the α8-α9 hairpin [Zhan *et al*., 1999]. In addition, there was a study suggesting that connecting-loop rigidity which is likely determined by two Pro residues (Pro^{43} and Pro^{47}) and the bulky side chains of other loop residues contributes to stability of the hairpin structure formed by two helices of the ATP synthase subunit *c* [Dmitriev & Fillingame, 2007]. According to a proposed mechanism of Cry toxin action that the toxins insert into the membrane as a helical hairpin formed by α4 and α5 [Gazit *et al*., 1998], the well-formed hairpin structure of these two helices is therefore required. Taken together, structural rigidity of the Pro-rich sequence (Pro^{193}Pro^{194}_Pro^{196}), a determinant of the α4-α5 loop stability, plays a crucial role in larvicidal activity of the Cry4Aa toxin, conceivably by supporting structure of the α4-α5 transmembrane hairpin.

3.1.3. Additional Role of Pro^{193} in Maintaining the Cry4Aa Structure

It is interesting to notice that among amino-acid replacements of the critical Pro residues (Pro^{193}, Pro^{194} and Pro^{196}) within the Cry4Aa α4-α5 loop, those of the Pro^{193} (P193V and P193G) had the most effect on larvicidal activity of toxin (**Fig. 4**). Consistently, data from alkaline solubilization showed that substitutions of Pro^{193} resulted in low solubility of the toxin inclusion while those of Pro^{194} and Pro^{196} retained the high level of solubility (**Fig. 3A**). Further structural characterization confirmed that mutations of Pro^{194} and Pro^{196} did not affect tertiary structure of the toxin molecule as the FPLC-purified trypsin-treated mutants, *i.e.* P194G and P196G, still exhibited similar intrinsic fluorescent spectra to that of the purified wild-type toxin (**Fig. 3B**).

Since a defect in alkaline solubility implies an insoluble aggregate form of the toxin resulted from protein misfolding, the great influence of Pro^{193} on inclusion solubility over the two other Pro residues (Pro^{194} and Pro^{196}) suggested an additional role of the Pro^{193} in structural arrangement of the toxin, apart from providing a structural rigidity. Interestingly, structural analysis of the Cry4Aa toxin revealed that C_α atom of the Pro^{193} points inwards towards the toxin molecule whereas those of Pro^{194} and Pro^{196} point outwards (**Fig. 5A**). Further structural analysis showed that replacements at position 193 resulted in a great change in interactions of the substituents with their neighboring residues, *i.e.*, P193G mutation introduced a cavity between the Gly^{193} and its surroundings, whereas P193V and P193F mutations caused a side-chain overlap effect (**Fig. 5B**). Altogether, optimal contact of Pro^{193} with its neighboring residues conceivably support the tertiary structure of the toxin, thus leading the Pro^{193} to be the most critical residue among Pro residues within the Cry4Aa α4-α5 loop.

3.1.4. Structure-Stability Relationships of the Long Cry4Aa α4-α5 Loop

As shown already, Pro-rich structure (Pro^{193}Pro^{194}_Pro^{196}) is essential for larvicidal activity of the Cry4Aa toxin. Further analysis *via* Pro-scanning mutagenesis of the loop residues (Ser^{191} to Asp^{200}) revealed that among Pro-substituted mutants, only S197P retained the high

level of toxicity (**Fig. 4**). Moreover, it was found that all the Pro-substituted mutations, except for N195P and S197P, affected inclusion solubility of the toxin. That means Pro residues are only acceptable at particular positions in the α4-α5 loop since existence of Pro at wrong positions may disturb overall structure of the protein as can be observed through a reduction in alkaline solubility.

As mentioned earlier, the α4-α5 loop of the Cry4Aa toxin is extraordinarily long (16 residues) when compared to those of other known Cry toxins (5-9 residues) (*see* **Fig. 1A**). Structural rigidity of the Pro-rich region which is currently shown to be required for the toxin activity may serve as a determinant for stabilizing such long loop. This notion becomes more possible as two other structural features of the loop are also found, *i.e.*, a disulfide bond (Cys^{192}-Cys^{199}) and a helical structure (Pro^{196} to Ile^{204}) (**Fig. 1C**), and the disulfide bond was previously shown to be essential for larvicidal activity of the Cry4Aa toxin [Tapaneeyakorn *et al*., 2005].

MD simulations of the Cry4Aa structure revealed that the α4-α5 loop has an RMSF value of 1.20 Å which is lower than those of the remaining loops within the pore-forming domain (**Fig. 6**). This data is consistent with that reported from previous simulations of the Cry4Aa trimer that the α4-α5 loop showed the lowest RMSF value among the domain-I loops [Taveecharoenkool *et al*., 2010]. As RMSF values indicate the intensity of fluctuation for each amino-acid residue, such RMSF data implied a substantial rigidity of the α4-α5 loop over the other loops with a similar or even a shorter length (α3-α4 loop: 12 residues; α5-α6 loop: 18 residues; α6-α7 loop: 12 residues) (**Fig. 6**). Remarkably, the α5-α6 loop which is only 2-residue longer than the α4-α5 loop showed the great RMSF value of 4.08 Å, indicating that this loop is incredibly unstable. It is interesting to note that the coordinates of part of this α5-α6 loop (Arg^{235} to Pro^{244}) were missing from the original X-ray crystal structure of the Cry4Aa toxin (PDB ID: 2C9K), thus supporting a great flexibility of this extra long loop. Compared to such flexible α5-α6 loop, the supreme stability of the Cry4Aa α4-α5 loop is relevant to its unique structure.

In conclusion, the data presented here revealed that structural rigidity of the α4-α5 loop plays an essential role in larvicidal activity of the Cry4Aa toxin, conceivably by maintaining hairpin structure of the α4-loop-α5 region. Such loop stability is contributed to a Pro-rich region together with a disulfide bond and a short helical structure exclusively found within the Cry4Aa α4-α5 loop. Currently, additional experiments are under the way to specify the function of the loop stability in biological activity of the Cry4Aa toxin, particularly in the step of membrane insertion.

3.2. Importance of Polarity of the α4-α5 Loop Residue—Asn^{166}

3.2.1. Larvicidal & Biochemical Characteristics of Cry4Ba-Asn^{166} Mutants

One biologically critical residue, i.e. Asn^{166} which is located within the loop connecting the transmembrane helices (α4 and α5) composing the pore-forming domain of the Cry4Ba toxin (**Fig. 7**) was previously identified by PCR-based directed mutagenesis [Kanintronkul *et al*., 2003]. Specific substitutions of Asn^{166} with polar uncharged or charged residues, *i.e.* Gln, Cys, Asp or Arg, could retain high toxicity against *A. aegypti* mosquito-larvae comparable to the wild type, whereas replacements with non-polar amino acids, *i.e*. Ala or Ile, almost totally abolished the larvicidal activity, suggestive of functional importance of the polarity of this α4-α5 loop residue [Kanintronkul *et al*., 2003]. In this report, toxin inclusions which were purified from particularly selected mutants, *i.e*. N166A, N166I and N166D (**Fig. 8A**, *inset*), were used instead to assess their relative toxicity. The data confirmed that the polarity of Cry4Ba-Asn^{166} placed within the α4-α5 loop is necessary for larvicidal activity (**Fig. 8A**).

As previously verified, the 130-kDa Cry4Ba protoxins of the wild type and the three mutants (N166A, N166I and N166D) were all cleaved by trypsin into two protease-resistant polypeptides of ~47 and ~20 kDa, in addition to the removal of ~65-kDa C-terminal half [Kanintronkul *et al*., 2003]. Herein, upon purification by size-exclusion FPLC chromatography, the trypsin-treated fragments (*i.e.* ~47 and ~20 kDa) of the three mutant toxins (**Fig. 8B**, *inset*) were found non-covalently associated with each other, forming a 65-kDa protein complex similar to the wild type under non-denaturing conditions used (50 mM Na_2CO_3/$NaHCO_3$, pH 9.0) and eluted from the column in a single peak corresponding to the retention time of the 66-kDa BSA protein marker.

To further determine if each substitution would induce structural changes in the Asn^{166} mutant proteins, the sum of the secondary structure components of the three FPLC-purified mutant toxins, N166A, N166I and N166D, were studied by far-UV CD spectroscopy in comparison with that of the purified wild-type toxin. As shown in **Fig. 8B**, all the CD spectral profiles are basically the same, validating that no drastic structural changes had occurred in consequence of these three mutations. This result is consistent with the data from toxin solubilization and trypsin-digesting susceptibility assays as demonstrated earlier, confirming that such mutations did not cause conformational changes of the N166A, N166I and N166D mutant proteins. These results verified that the loss in larvicidal activity observed for both N166A and N166I mutants (**Fig. 8A**) are least likely to be due to protein misfolding after substitutions with either of these two hydrophobic side-chains.

3.2.2. Membrane Permeability of Dye-Loaded LUVs by Cry4Ba & Its Mutants

To examine the effect of the Cry4Ba-Asn^{166} mutant toxins on membrane permeability, encapsulated calcein-leakage assays were employed to assess the toxin-induced permeabilization of LUVs whose composition used (PC/PE/Ch, 10:10:1 weight ratio) is similar to

insect cell membranes. Release of the entrapped calcein by individual tested toxins was semi-empirically quantified as the relative increase in fluorescence de-quenching intensity (**Fig. 9**).

Release activity of the 65-kDa purified wild-type toxin against the calcein-loaded LUVs was at first evaluated at different protein concentrations, and the concentration-versus-release activity profile was generated (**Fig. 9A**). The leakage of trapped calcein increased sigmoidally with toxin concentration, *i.e.* only a small release was observed at low concentrations, but then rather steeply at higher concentrations. This indicates that LUVs were not permeabilized until a critical toxin monomer/vesicle ratio was accomplished. Kinetics of toxin-pore formation are reflected in the dependence of fractional activity (Y) on the Cry4Ba toxin concentration as described in the logarithmic form of the Hill equation, $\log Y = n \log [T] - \log EC_{50}$. The Hill coefficient ($n$) for the tested toxin was determined by fitting the nonlinear concentration-activity profile into the Hill equation (**Fig. 9A**, *inset*). For the 65-kDa Cry4Ba activated toxin in LUVs, at pH 9.0, the value of n was found to be about 1.3. Thus, it would conceivably require more than one molecule of the activated toxin to form a functional pore structure in this insect mimetic liposome. It was observed previously that a mixture of Cry4Ba toxin monomers, dimers and trimers is present in liposomes, whereby trimeric species predominantly appear after prolonged incubation of toxin-lipid vesicle [Likitvivatanavong *et al.*, 2006]. The present results are also in agreement with our previously reported electron crystallographic data at 17 Å resolution, which demonstrated a horizontal arrangement of three Cry4Ba molecules per membrane-associated pore complex in 2D (two-dimensional) crystals [Ounjai *et al.*, 2007].

In addition, the effective toxin concentration required for 50% dye release (EC_{50}) was also obtained from the curve fitted to the Hill equation. The calculated EC_{50} value for the Cry4Ba wild-type toxin against the calcein-loaded vesicles was found to be ~0.95 μM, which is comparable to that of the larvicidal-active N166D mutant, as both were observed within 10 min (**Fig. 9**, **A** & **B**). However, both larvicidal-inactive mutants, N166A and N166I (at concentrations of 0.95 μM or ~60 μg/ml) were much less active in inducing the leakage of the calcein-loaded vesicles, with a maximally observed release of only 20% (**Fig. 9**, **C** & **D**), whereas the control showed no effect on dye-leakage (**Fig. 9**, **E**), indicating that the leakage of calcein did not occur as a result of instability of the vesicle membrane. Taken together, the results substantiate that the polarity of this α4-α5 loop residue–Asn^{166} is required for membrane-pore formation, and therefore a prerequisite for larvicidal activity (*see* **Fig. 8A**).

3.2.3. Ion-Channel Characteristics Formed by Cry4Ba & Its Asn^{166}-Mutants

Further attempts were made to determine if each single-mutation at Asn^{166} causes an adverse effect on the toxin ability to form ion channels on PLBs. Under symmetrical ionic conditions (at 150 mM KCl, 10 mM Tris-HCl, pH 8.5), the Cry4Ba wild-type and all three mutants (at doses of 0.3 μM or ~20 μg/ml) were able to induce single channel currents at

voltages between −100 and +100 mV, as shown by representative current traces in **Fig. 10A**. However, the capability to produce ion channels was found to be reduced in the two non-toxic mutant proteins, *i.e*. N166A, and N166I, but not in the larvicidal-active N166D mutant, as compared with the wild-type toxin. In agreement with previous reports of ours on Cry4Ba and other workers on Cry toxins [Grochulski *et al*., 1995; Slatin *et al*., 1990; Peyronnet *et al*., 2002; Puntheeranurak *et al*., 2004; Kao *et al*., 2011], several distinct sub-conductance levels were frequently detected for all tested toxins. These observations are suggestive of a multimeric manner of toxin incorporation into the lipid bilayer. Like other ion channels [Bali & Akabas, 2012; Horrigan, 2012], the Cry toxin-induced channels would perhaps go through conformational rearrangements during channel gating. Although at present a possible gating mechanism for the channels induced by Cry toxins has not yet been unambiguously demonstrated, PLB experiments suggest that, in analogy to known channel-forming toxins [Marchioretto *et al*., 2013], Cry toxin-induced channels could exhibit closed and open functional states [Grochulski *et al*., 1995; Slatin *et al*., 1990; Peyronnet *et al*., 2002; Puntheeranurak *et al*., 2004; Kao *et al*., 2011].

As shown in **Fig. 10B**, the current-voltage relations of all single channels formed by the wild-type and mutant toxins are linear revealing maximum conductances ranging from ~150 to ~450 pS. Consistent with the dye-leakage results, the maximum conductance of the bio-active N166D mutant (425.5 ± 6.5 pS, n = 4) was found to be comparable to that of the wild-type toxin (450.5 ± 25.5 pS, n = 4). However, both the non-toxic mutants, N166A and N166I, exhibited about a half lower conductance (165.0 ± 5.5 pS, n = 5 and 205.5 ± 14.5 pS, n = 4, respectively). These results suggest that the α4-α5 loop residue (Asn^{166}) is involved in regulating the passage of ions through the channel pore. The data also imply that the polarity but not the type of amino acid side-chain at position-166 is an important determinant for ion permeation and conduction in the Cry4Ba-induced channels.

3.2.4. Structure & Dynamics of Cry4Ba α4-α5-Induced Pore Models in Bilayers

Currently, the number of toxin monomers that constitute a functional pore complex within the lipid membrane is still under debate. Previous studies have reported the existence of trimeric as well as tetrameric complexes of toxin monomers [Puntheeranurak *et al*., 2005; Ounjai *et al*., 2007; Muñóz-Garay *et al*., 2009; Groulex *et al*., 2011]. A trimeric organization of the 65-kDa activated Cry4Ba toxin in association with lipid membranes as revealed by 2D crystallographic analysis was described recently [Ounjai *et al*., 2007]. Here we performed MD simulations of a trimeric α4-α5 pore of Cry4Ba and its three Asn^{166} mutants (N166A, N166I and N166D) in a DMPC bilayer for 60 ns to study their conformational dynamics. During the simulation-time interval of 60 ns, the wild-type pore visibly opened up as shown in **Fig. 11**, **A-D**. By simple geometry, the pore diameter (D) at time t = 60 ns could be estimated from the average separation distance d ~25 Å, as $D = d/\sqrt{3} \approx 25/\sqrt{3} \approx 14.4$ Å. The calculated pore size is large enough for calcein, a water-soluble dye with a hydrodynamic-Stokes diameter of ~13 Å to pass

through as demonstrated above in the dye-leakage experiments (*see* **Fig. 9**). The data are also in agreement with a pore diameter of ~20 Å as estimated from polyethylene glycol-blockage PLB experiments for Cry1Ca [Peyronnet *et al*., 2002].

Initial size and dynamics of the trimeric pores formed by the wild type and its mutants were obtained from their alterations in the average separation distance *d* (C_α to C_α) between three Asn^{166} residues on each individual pore (**Fig. 11E**). It can be seen that the trimeric pores of N166A and N166I mutants did not open up, while that of N166D opened more but still less than that of the wild type. This open-pore structure could possibly be prevented by unwanted hydrophobic interactions between the three individual mutated residues (*i.e.* Ala or Ile). To explain what caused the wild-type Cry4Ba pore to open, we examined molecules that interact with the three Asn^{166} side-chains on the loops of individual α4-loop-α5 hairpins. It was found that these three side-chains interact with the polar head groups of DMPC lipids as well as water molecules. The partial negative charge (negative dipole) of oxygen atoms (color in red) on Asn^{166} could attract the positively charged choline moiety of DMPC lipids (**Fig. 12, A & B**). Such protein-lipid interactions could thus trigger the opening of the pore.

The number of lipids within 4 Å of the three Asn^{166} residues and their corresponding mutated side-chains were also analyzed (**Fig. 12C**). It can be seen that both wild-type and N166D pores exhibit an increased number of lipid molecules interacting with them (up to four and two lipids, respectively), while pores containing N166A and N166I have a lower number of lipid molecules around the mutated side-chains (between zero and one). This would indicate that the polarity at the α4-α5 loop position-166 plays an important role in protein-lipid interactions and hence for Cry4Ba-pore opening at the membrane-water interface. As can be also inferred from the Cry4Ba-pore model, Asn^{166} basically faces the pore lumen and the interfacial regions of the membrane. Therefore, substitutions with a non-polar residue could directly affect its interactions with surrounding water and lipids, thus having an adverse effect on conformational changes.

In conclusion, our present results provide more insight into the functional significance of the α4-α5 loop residue–Asn^{166} within the Cry4Ba pore-forming domain. We have demonstrated that the polarity of Cry4Ba-Asn^{166} is essentially involved in ion permeation through the toxin-induced pore and likely promotes the toxin-pore opening. Further studies on toxin-induced pore architecture and mechanism of ion passage through the channel pore would be of great interest. A detailed understanding of structural basis for ion permeable-pore formation by this mosquito-active toxin is very imperative since this will bolster the development of engineered biopesticides for the control of human-disease vectors.

Table 1: Complementary primers for the generation of Cry4Aa mutant toxins

Primer	Sequence[a]	Restriction site
P193G-f	5′-AAACTCTTGT**GGG**CC**C**AATCCTAGTGATTG-3′	*Hae*III
P193G-r	3′-GAACATTTGAGAACA**CCC**GG**G**TTAGGATCAC-5′	
P194G-f	5′-TTGTCC**GGG**TAATCCTAGTGATTG-3′	*Hpa*II
P194G-r	3′-CATTTGAGAACAGG**CCC**ATTAGGAT-5′	
P196G-f	5′-TCCTAAT**GGATC**TGATTGCGATTACTA-3′	*Sau*3AI
P196G-r	3′-GAACAGGAGGATTA**CCTAG**ACTAACG-5′	
P193V-f	5′-CTCTTGT**GTA**CCTAATCCTAGTGA-3′	*Rsa*I
P193V-r	3′-GAACATTTGAGAACA**CAT**GGATTAG-5′	
P194V-f	5′-CTTGTCC**GGT**TAATCCTAGTGATTG-3′	*Hpa*II
P194V-r	3′-CATTTGAGAACAGG**CCA**ATTAGGAT-5′	
P196V-f	5′-CTCCTAAT**GTCTCA**GATTGCGATTACTATAAC-3′	*Dde*I
P196V-r	3′-TGAGAACAGGAGGATTA**CAGAGT**CTAACGC-5′	
P193F-f	5′-AGCTTGTAAAC**AGC**TGT**TT**TCCTAATCCTAGTG-3′	*Pvu*II
P193F-r	3′-GTCTCGAACATTTG**TCG**ACA**AA**AGGATTAGGAT-5′	
S191P-f	5′-AGCTTGT**T**AAC**C**CTTGTCCTCCTAATC-3′	*Hinc*II
S191P-r	3′-GTAAGGTCTCGAACA**A**TTG**G**GAACAGG-5′	
C192P-f	5′-AGCTTGT**T**AACTCT**CC**TCCTCCTAATCCTAGTG-3′	*Hinc*II
C192P-r	3′-CAGTAAGGTCTCGAACA**A**TTGAGA**GG**AGGAGG-5′	
N195P-f	5′-TCCTCCT**CCC**CC**G**AGTGATTGCGATTACTA-3′	*Ava*I
N195P-r	3′-TTTGAGAACAGGAGGA**GGG**GG**C**TCACTAAC-5′	
S197P-f	5′-CTAATCCT**CCG**GATTGCGATTACTATA-3′	*Hpa*II
S197P-r	3′-CAGGAGGATTAGGA**GGC**CTAACGC-5′	
D198P-f	5′-CTCCTAA**C**CC**G**AGT**CC**TTGCGATTACTATAACATAC-3′	*Ava*I
D198P-r	3′-ATTTGAGAACAGGAGGATT**G**GG**C**TCA**GG**AACGCTA-5′	
C199P-f	5′-CTAGTGAT**CC**CGATTACTATAACAT-3′	*Dpn*I
C199P-r	3′-GATTAGGATCACTA**GG**GCTAATGA-5′	
D200P-f	5′-TGATTGC**CG**TACTATAACATACTAG-3′	*Rsa*I
D200P-r	3′-TAGGATCACTAACG**GGC**ATGATATTG-5′	

[a] Recognition sites introduced for restriction enzyme analysis are underlined. Bold letters indicate mutated nucleotide residues; f and r represent forward and reversed primers, respectively.

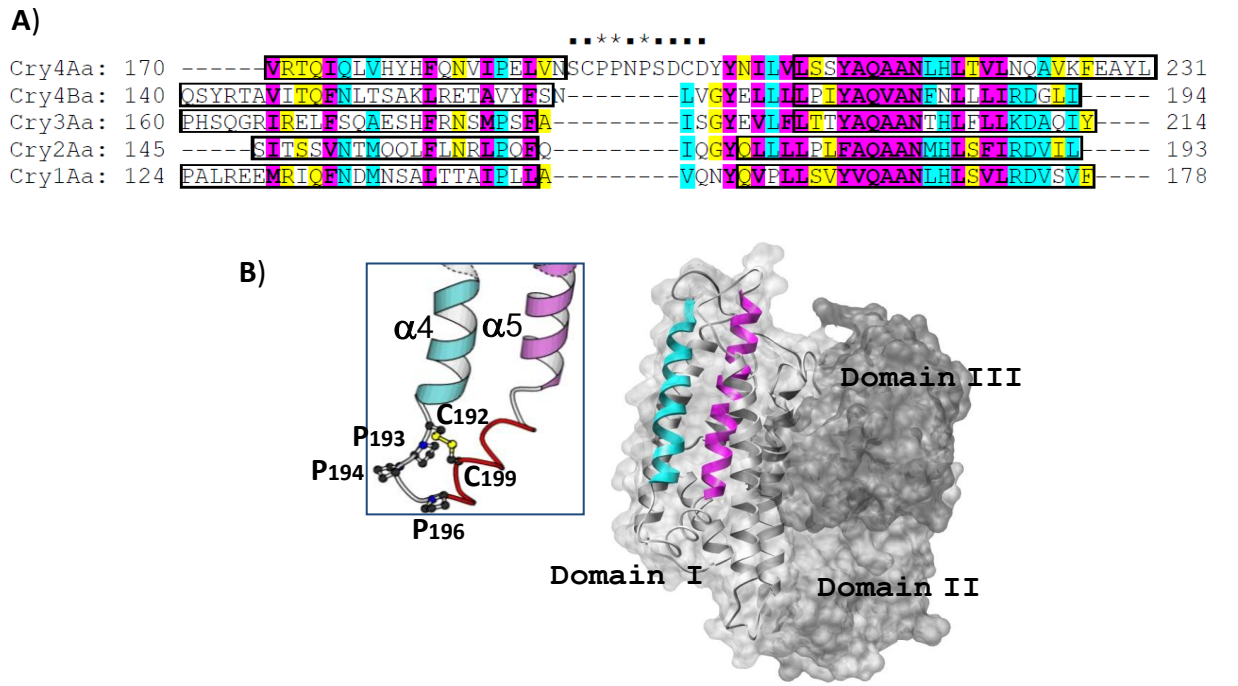

Figure 1: (A) Multiple sequence alignment of α4-loop-α5 of the Cry4Aa toxin with those of other known Cry toxins, Cry1Aa, Cry2Aa, Cry3Aa and Cry4Ba. Sequences with helical structure are in the boxes. The critical proline residues and other mutated loop residues are indicated by * and ■, respectively. (B) Crystal structure of the activated Cry4Aa toxin, showing the three-domain organization; domain I with the of α4-α5 transmembrane hairpin (schematic ribbon) and domains II-III (surface model). Inset, The α4-α5 loop with three critical Pro residues (Pro^{193}, Pro^{194} and Pro^{196}), a disulfide bridge (Cys^{192}-Cys^{199}) and a short helical structure (shown as red backbone trace).

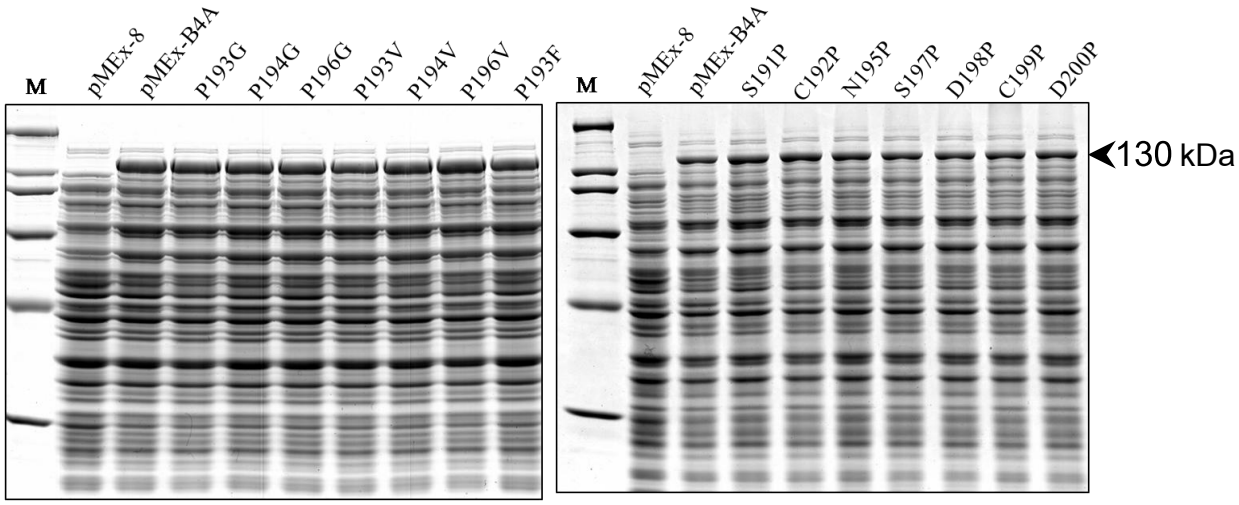

Figure 2: SDS-PAGE (Coomassie brilliant blue-stained 10% gel) analysis of lysates extracted from *E. coli* (10^7 cells) expressing 130-kDa protoxins of Cry4Aa wild-type (pMEx-B4A) or its mutants. *E. coli* cells harboring pMEx-8 vector were used as a negative control. (M) represents the molecular standards.

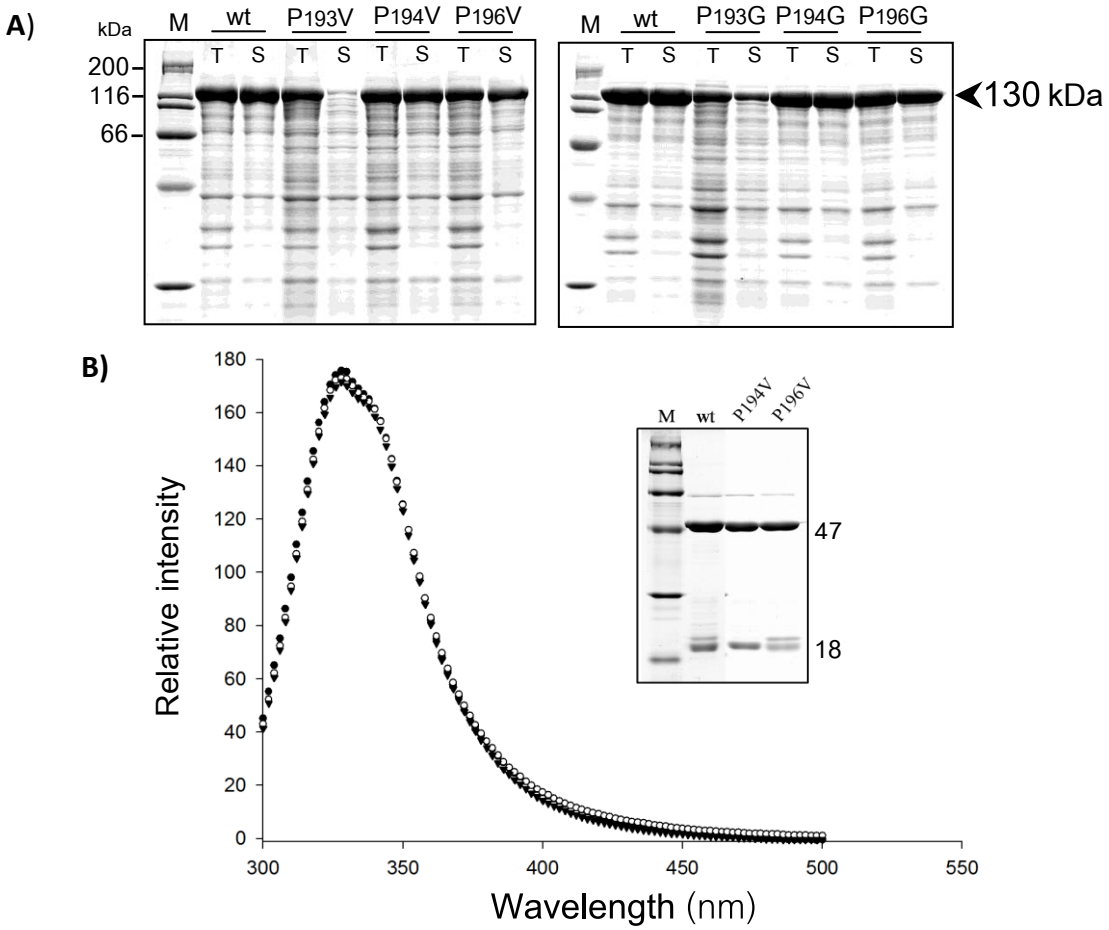

Figure 3: (**A**) SDS-PAGE (Coomassie brilliant blue-stained 10% gel) analysis of solubility of the Cry4Aa wild-type (wt) or its mutant toxin inclusions (P193G, P194G, P196G, P193V, P194V and P196V) in carbonate buffer, pH 9.0. T and S represent total fractions and an equal volume of the supernatants after centrifugation, respectively. M represents the molecular mass standards. (**B**) Fluorescence emission spectra of the purified Cry4Aa wild-type (●) on excitation of 280 nm in comparison with that of the mutant toxins, P194G (○) and P196G (▼). Inset, SDS-PAGE analysis of the purified trypsin-treated toxins (wild-type, P194G and P196G) that are composed of 47- and 18-kDa fragments.

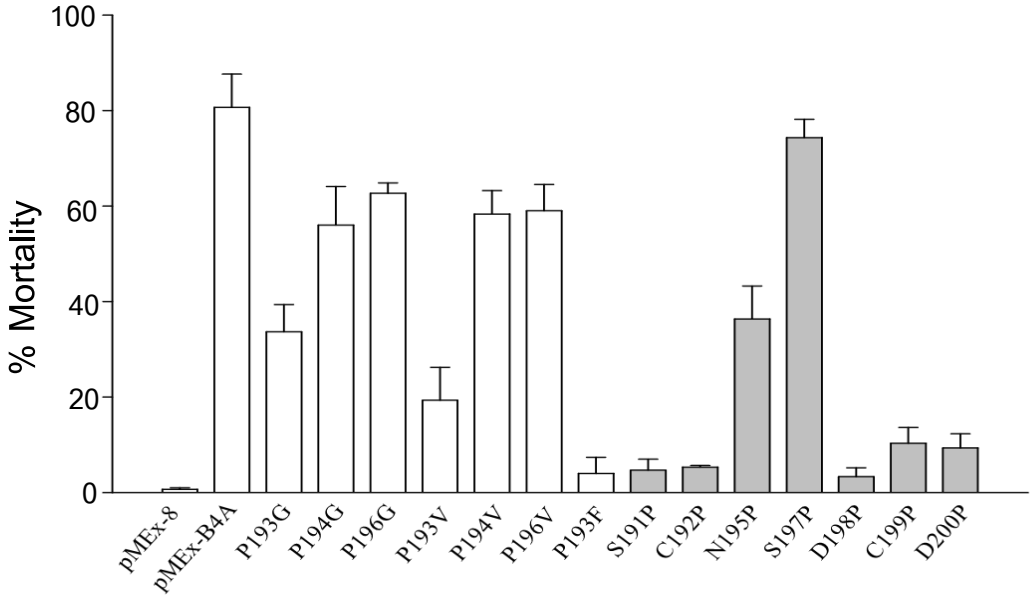

Figure 4: Toxicity of *E. coli* cells expressing the Cry4Aa wild-type (pMEx-B4A) or its loop mutants against *A. aegypti* larvae. *E. coli* cells harboring the pMEx-8 vector were used as a negative control. Error bars indicate standard errors of the mean from three independent experiments.

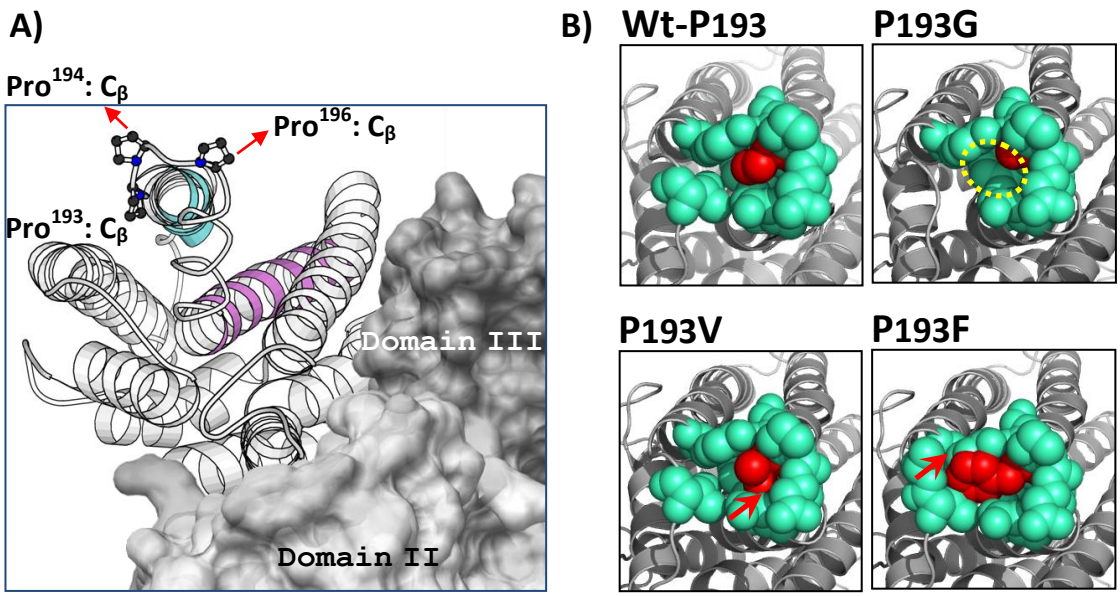

Figure 5: Bottom views of part of the Cry4Aa structure, showing (**A**) directions of C_β atoms of each Pro side chain in the α4-α5 loop and (**B**) interactions between residues at the critical position 193 within the α4-α5 loop (shown as red space-filling model) and their neighboring residues within 5 Å (green cyan space-filling model). The cavity introduced inside the interaction is encircled. The red arrows indicate the side-chain overlap.

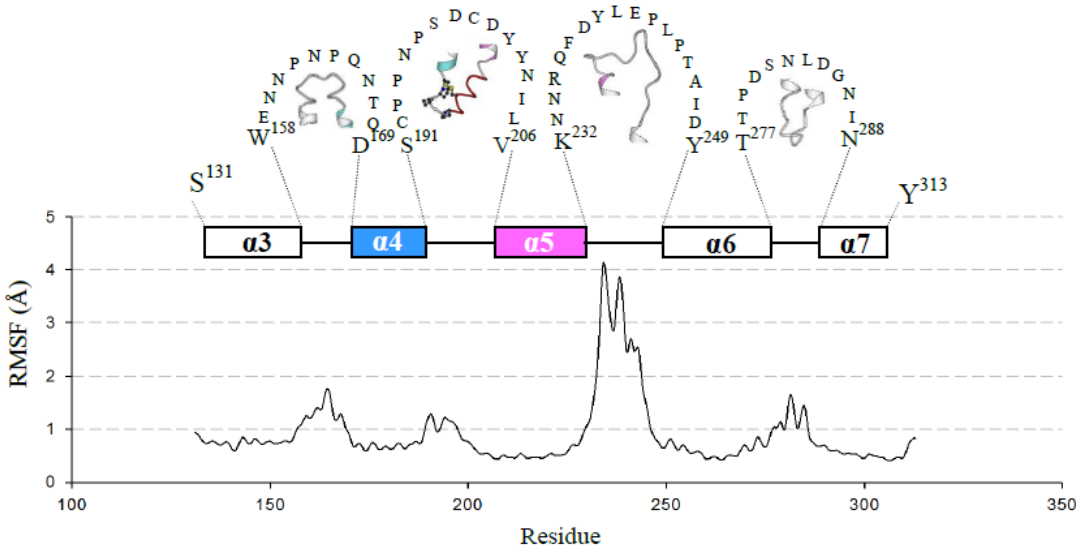

Figure 6: The C_α RMSF of pore-forming domain of the Cry4Aa toxin during MD simulations. α-helices are illustrated as rectangles. Loops connecting each two adjacent helices are shown as 1-letter amino-acid sequences. Conformations of each loop were shown under the corresponding sequences.

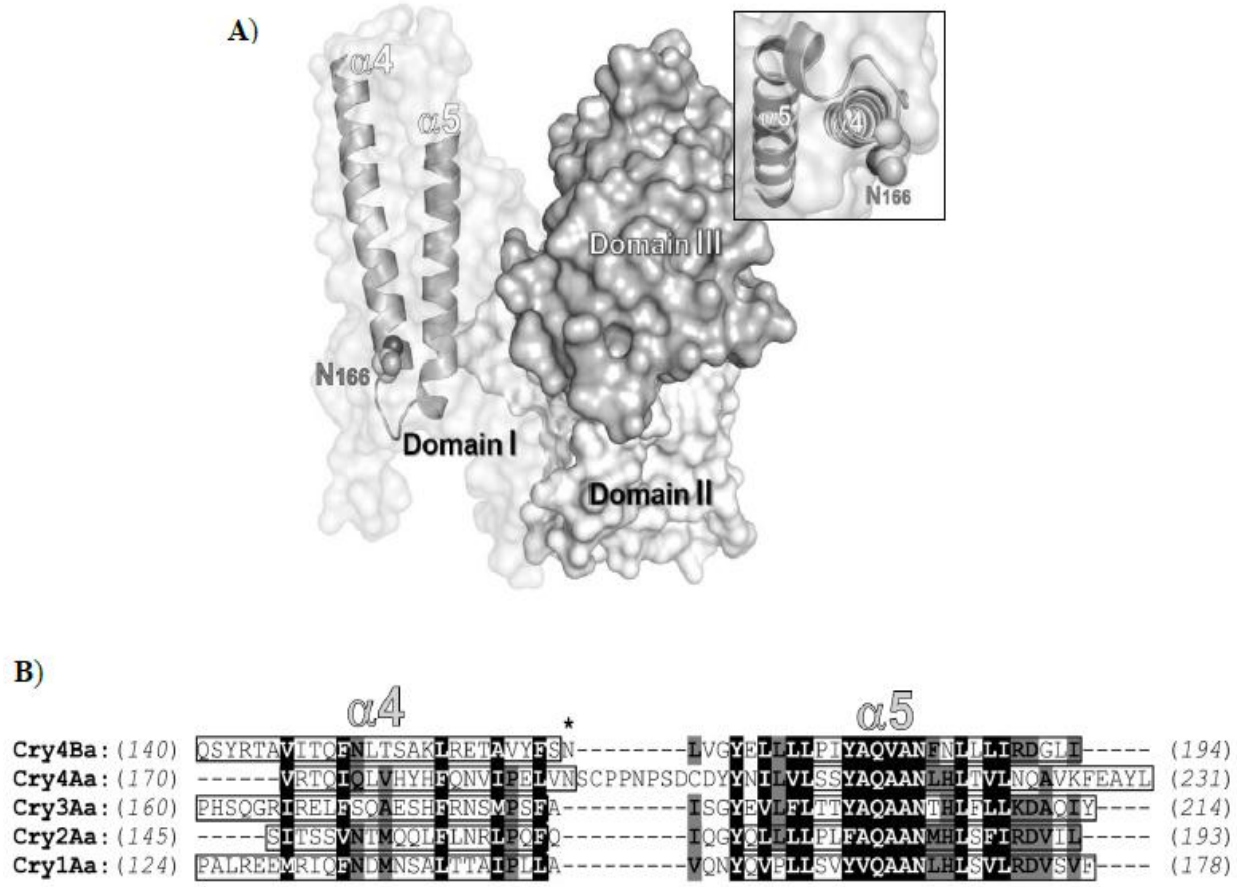

Figure 7: The Cry4Ba crystal structure and its Asn[166] location. (*A*) Surface representation of the three-domain Cry4Ba toxin organization (domains I-III), illustrating the α4-loop-α5 hairpin (schematic ribbon) within the pore-forming domain (domain I) with the location of Asn[166] drawn as vdW (van der Waals) spheres. Inset, a zoom-in bottom view of the exposed Asn[166] residue. The structure was generated by using PyMOL program. (*B*) Sequence alignments of the α4-loop-α5 hairpin of Cry4Ba with those of four other known Cry structures, Cry4Aa, Cry3Aa, Cry2Aa and Cry1Aa. Corresponding α4 and α5 of all known structures are illustrated as rectangular blocks connected by loop sequences. Note that the position of Cry4Ba-Asn[166] (denoted by *) corresponds most closely to that of Cry4Aa-Asn[190] which was previously substituted with Ala, but showing no effect on the toxin activity [Pornwiroon *et al*., 2004]. .

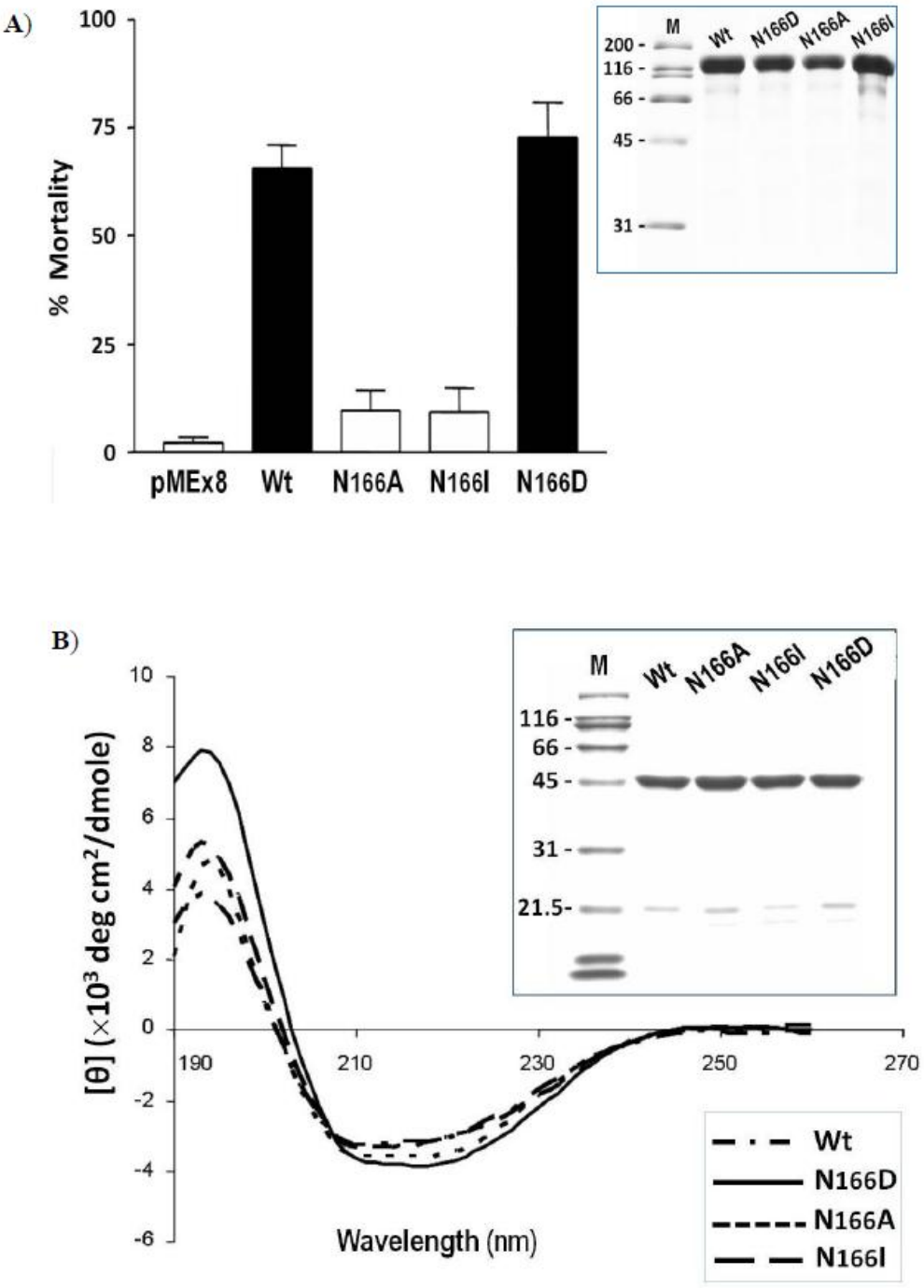

Figure 8: Larvicidal and biochemical features of Cry4Ba-Asn[166]-mutants. (*A*) Comparison of larvicidal activities between the Cry4Ba wild-type (Wt) and its Asn[166] mutant toxins (N166A, N166I, N166D) against *A. aegypti* mosquito-larvae using purified inclusions (5 µg/ml). pMEx8 represents a negative control: *E. coli* lysate containing the plasmid vector. Error bars indicate standard errors of the mean from at least three independent experiments. Inset, SDS-PAGE analysis of purified inclusions, showing 130-kDa wild-type and its mutant protoxins (5 µg/lane). M, molecular mass standards. (*B*) CD spectra of the 65-kDa purified Cry4Ba toxin in comparison with that of the three mutants, N166A, N166I and N166D. Inset, SDS-PAGE analysis of the 65-kDa Cry4Ba wild-type and its mutant toxins after trypsin activation and FPLC-purification, showing two non-covalently associated fragments of ~47 and ~20 kDa.

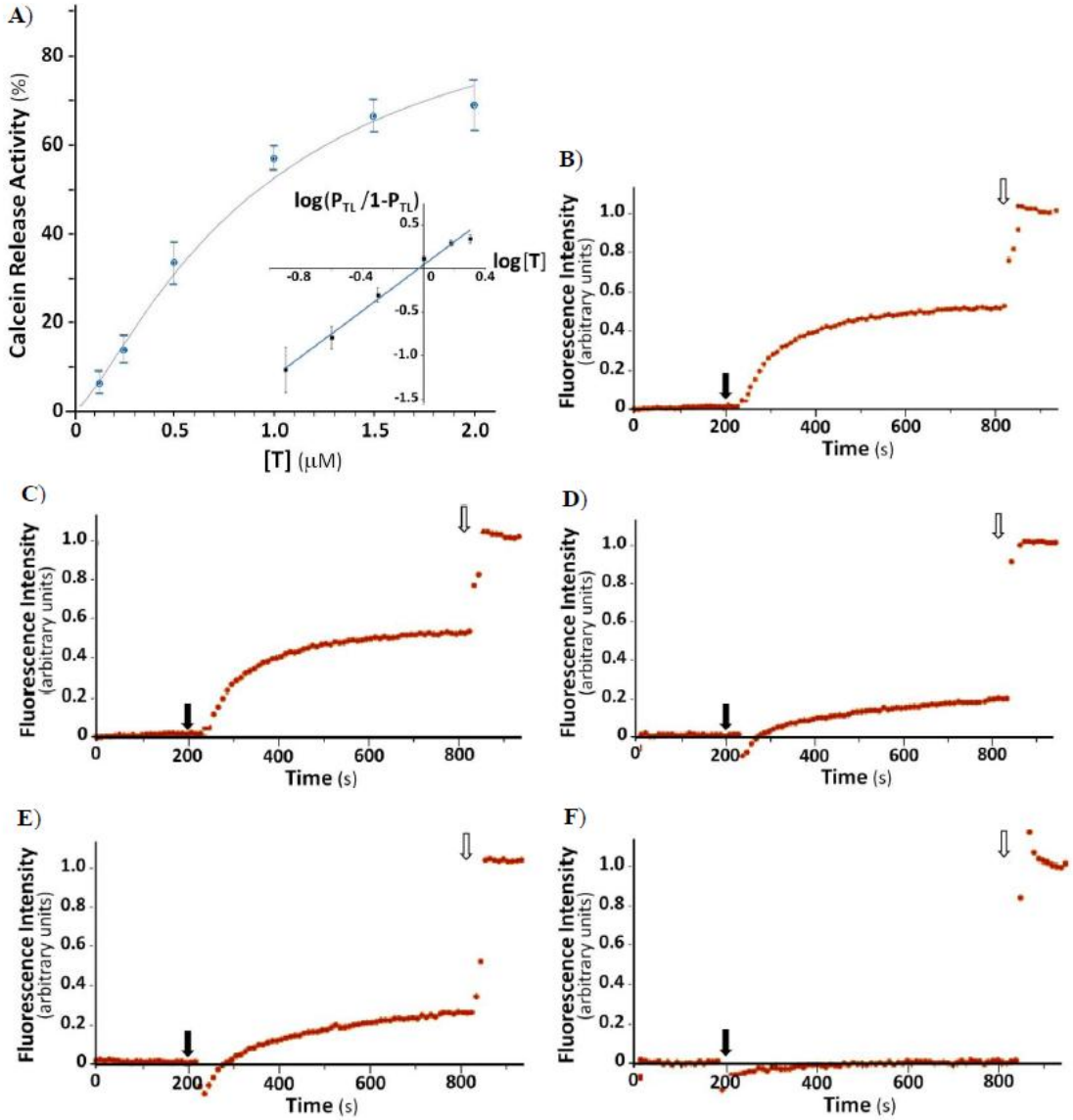

Figure 9: Effect on membrane permeability of calcein-loaded liposomes by Cry4Ba and its Asn^{166}-mutants. (*A*) Dose response curve for membrane permeability induced by the 65-kDa Cry4Ba wild-type toxin. Inset, the plot of fractional release activity *Y* (P_{TL} /1 — P_{TL}) versus toxin concentration [T]. Error bars indicate standard errors of the mean from two independent experiments. (*B-F*) Traces represent fluorescence intensity as function of time *t* after adding Cry4Ba or its Asn^{166} mutants (60 μg/ml). The maximum release was obtained by adding 0.1% triton X-100 (white arrows) after 10 min-incubation with individual tested toxins (black arrows); (*B*) Cry4Ba wild type, (*C*) N166D, (*D*) N166I, (*E*) N166A, or (*F*) the carbonate buffer (negative control).

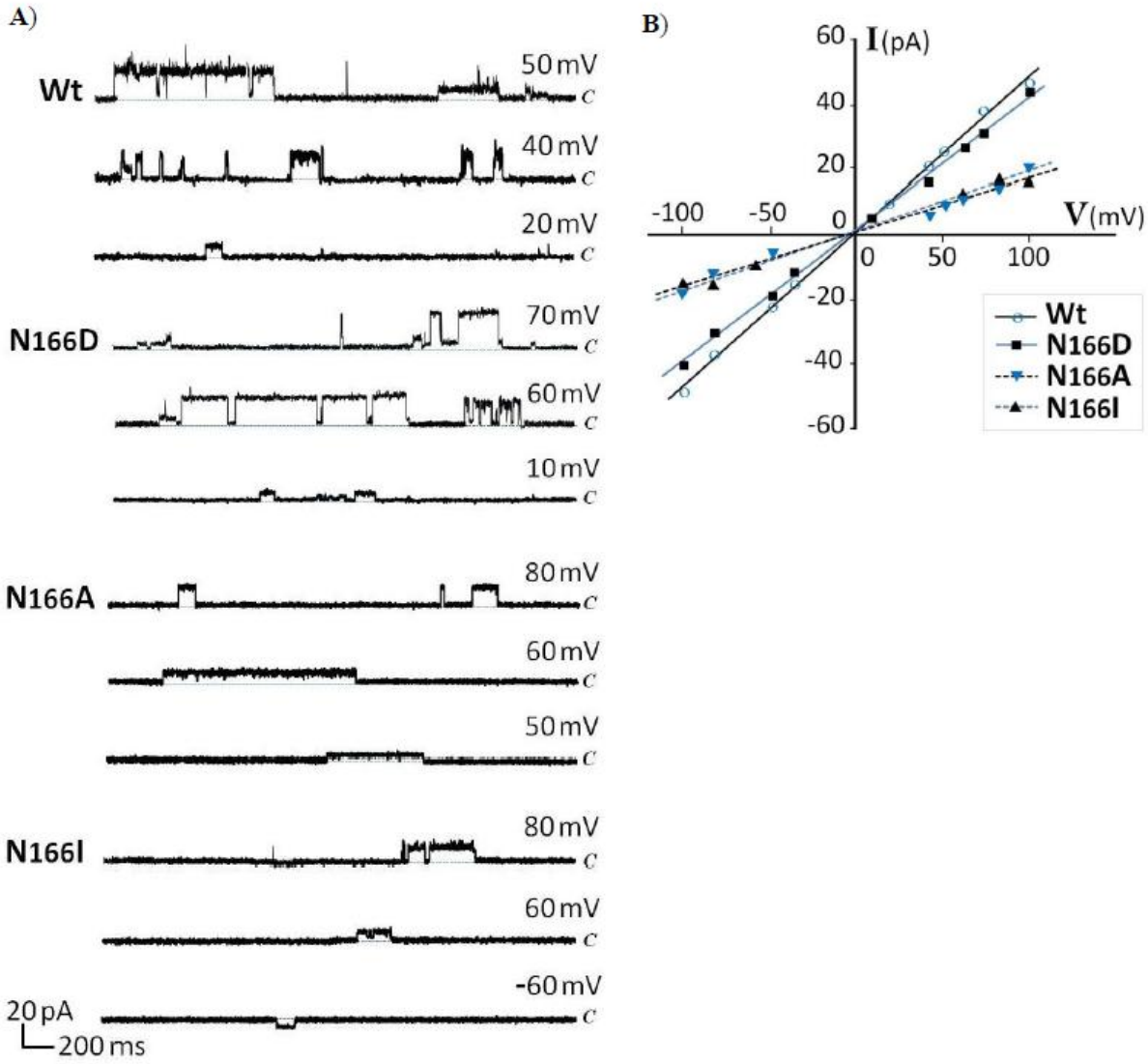

Figure 10: Ion-channel properties of Cry4Ba and its Asn^{166}-mutant toxins. (*A*) Current traces recorded after partition of the 65-kDa purified Cry4Ba wild-type (Wt) and its mutant toxins—N166D, N166A and N166I (20 µg/ml) into PLBs under symmetrical conditions (150:150 mM KCl *cis:trans*). Applied voltages are indicated on the right side of each trace. The close stage level of the channel is denoted by letter *c*. Vertical and horizontal bars indicate measured current-time scales, respectively. (*B*) Current-voltage relations obtained from the single-currents recorded under symmetric conditions.

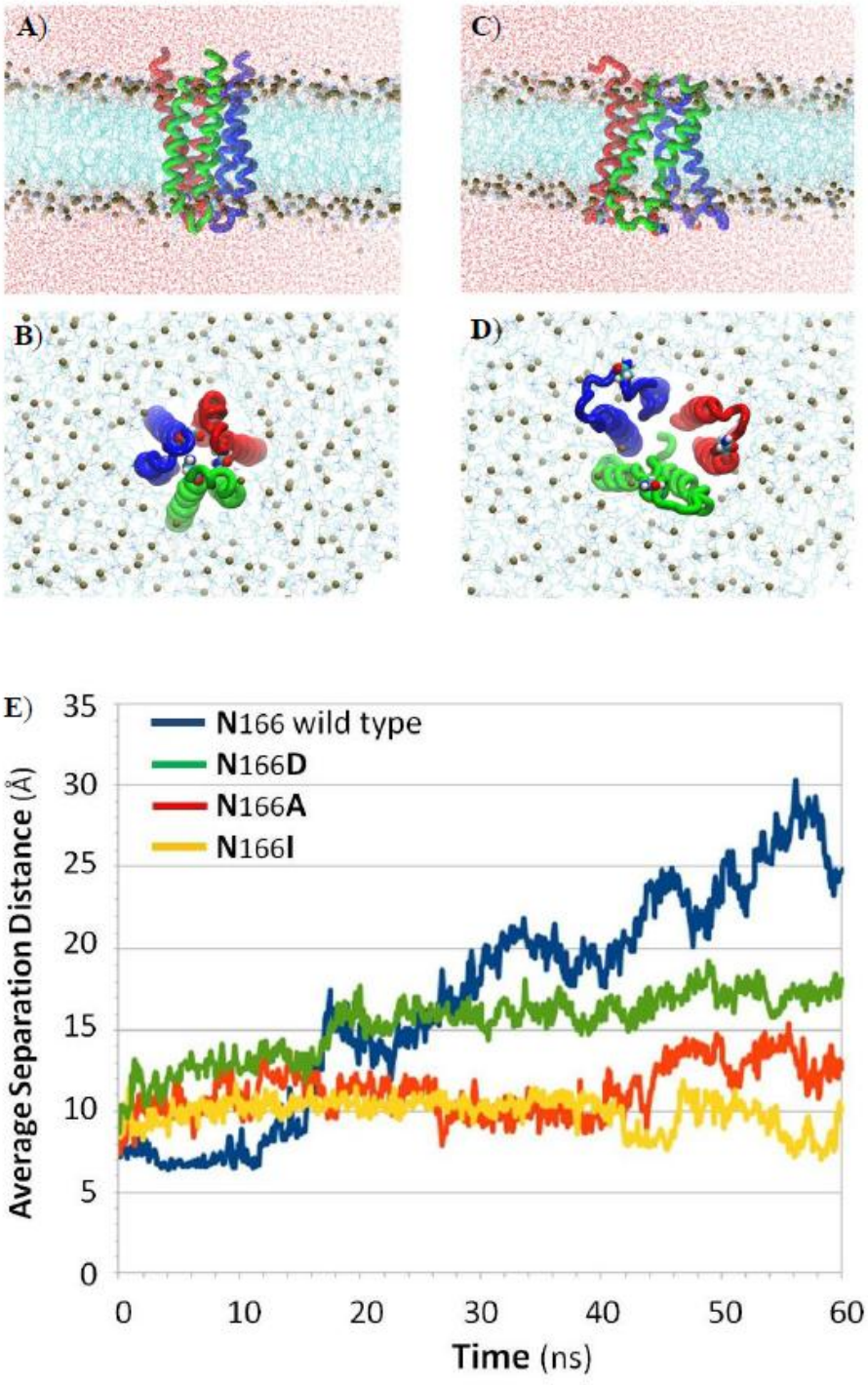

Figure 11: Opening of the trimeric Cry4Ba pore during 60-ns MD simulations. Snapshots of the MD trajectories (side and bottom views) at time *t* = 0 ns (*A* and *B*) and at time *t* = 60 ns (*C* and *D*). Three α4-α5 hairpins are rendered as tubes. Three Asn^{166} residues and phosphorus atoms of DMPC lipids are drawn as vdW spheres. DMPC lipids (cyan) and water (red) are shown as lines. (*E*) Average separation distance (C_α to C_α) between three Asn^{166} residues on the trimeric Cry4Ba pore and its mutants versus time during 60-ns MD simulations.

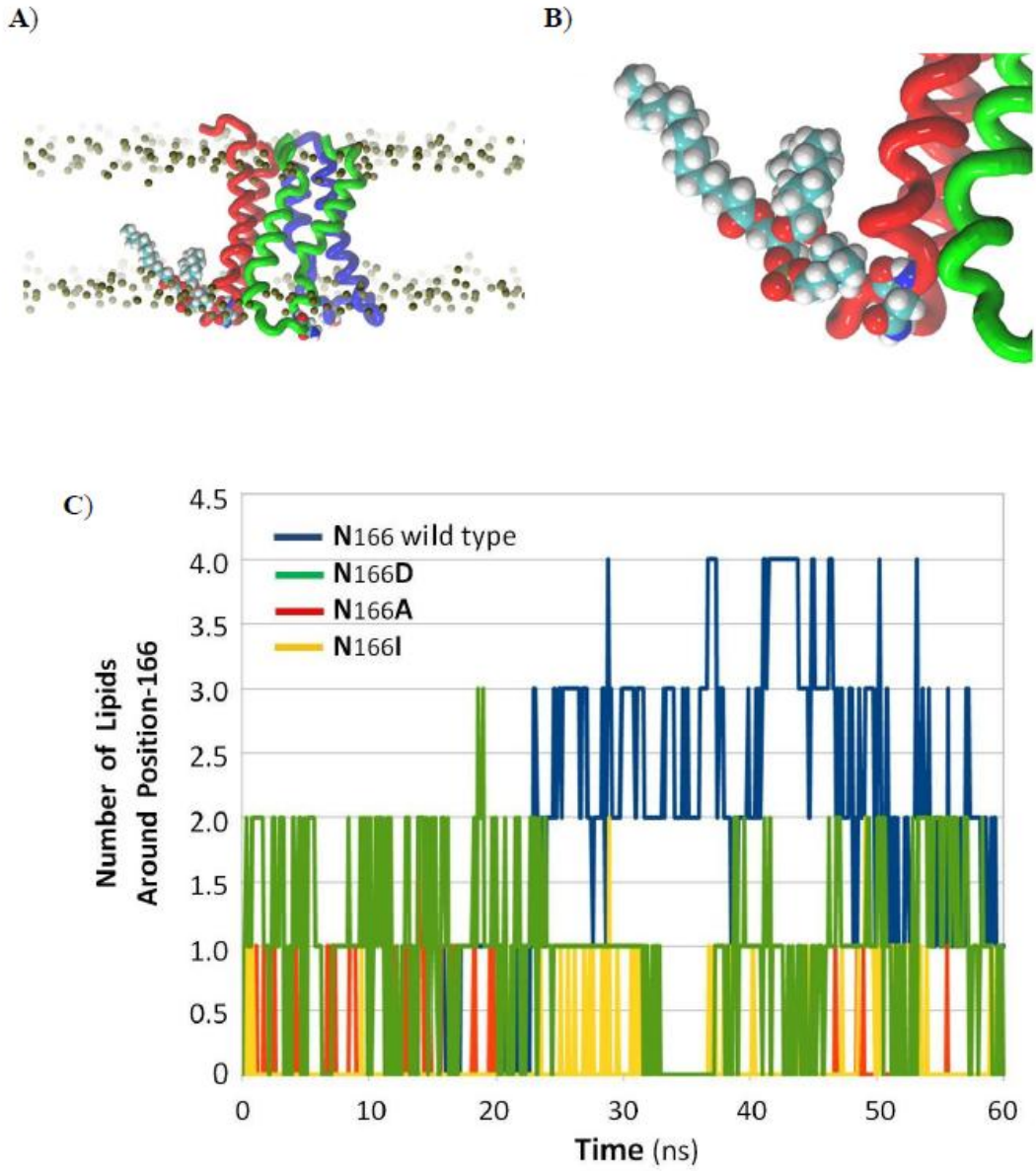

Figure 12: Interactions between Cry4Ba-166 side chains and DMPC-polar head groups. (*A*) DMPC lipids within 4 Å of one of Asn^{166} residues on Cry4Ba pore relative to phosphorus layers (gold spheres) of DMPC membrane at time t = 60 ns. For clarity, lipids and water are not shown. (*B*) Magnified view of the DMPC lipid interacting with an Asn^{166} residue of the Cry4Ba pore. Both Asn^{166} residues and the DMPC lipid are rendered as vdW spheres and colored by atom names. (*C*) Number of DMPC lipids within 4 Å of three Asn^{166} residues and their mutants on the trimeric Cry4Ba pore versus time during 60-ns MD simulations.

4. References

Angsuthanasombat, C. (2010) *Open Toxinol. J.* **3**, 119-125.

Bali, M., and Akabas, M. H. (2012) *J. Biol. Chem.* **287**, 27762-27770.

Boonserm, P., Davis, P., Ellar D. J., and Li, J. (2005) *J. Mol. Biol.* **348**, 363-382.

Boonserm, P., Mo, M., Angsuthanasombat, C., and Lescar, J. (2006) *J. Bacteriol.* **188**, 3391-3401.

Chen, X. J., Curtiss, A., Alcantara, E., and Dean, D. H. (1995) *J. Biol. Chem.* **270**, 6412-6419.

Dmitriev, O.Y., and Fillingame, R.H. (2007) *Protein Sci* **16**, 2118-2122.

Federici, B. A., Park, H.-W., and Bideshi, D. K. (2010) *Open Toxinol. J.* **3**, 83-100.

Gazit, E., La Rocca, P., Sansom, M. S., and Shai, Y. (1998) *Proc. Natl. Acad. Sci. U.S.A.* **95**, 12289-12294.

Gerber, D., and Shai, Y. (2000) *J. Biol. Chem.* **275,** 23602-23607.

Grochulski, P., Masson, L., Borisova, S., Pusztai-Carey, M., Schwartz, J. L., Brousseau, R., and Cygler, M. (1995) *J. Mol. Biol.* **254**, 447-464.

Groulex, N., McGuire, H., Laprade, R., Scheartz, J. L., and Blunck, R. (2011) *J. Biol. Chem.* **286**, 42274-42282.

Horrigan, F. T. (2012) *J. Gen. Physiol.* **140**, 625-634.

Kanintronkul, Y., Sramala, I., Katzenmeier, G., Panyim, S., and Angsuthanasombat, C. (2003) *Mol. Biotechnol.* **24**, 11-20.

Kao, C.-Y., Los, F. C. O., Huffman, D. L., Wachi, S., Kloft, N., et al. (2011) *PLoS Pathog*. **7**, e1001314.

Leetachewa, S., Katzenmeier, G., and Angsuthanasombat, C. (2006) *J. Biochem. Mol. Biol.* **39**, 270-277.

Li, J., Carroll, J., and Ellar, D. J. (1991) *Nature* **353**, 815-821.

Likitvivatanavong, S., Katzenmeier, G., and Angsuthanasombat, C. (2006) *Arch. Biochem. Biophys.* **445**, 46-55.

Masson, L., Tabashnik, B. E., Liu, Y. B., Brousseau, R., and Schwartz, J. L. (1999) *J. Biol. Chem.* **274**, 31996-32000.

Marchioretto, M., Podobnik, M., Serra, M. D., Anderluh, G. (2013) *Biophys. Chem.* doi:10.1016/j.bpc.2013.06.015.

Morse, R. J., Yamamoto, T., and Stroud, R. M. (2001) *Structure* **9**, 409-417.

Muñóz-Garay, C., Portugal, L., Pardo-López, L., Jiménez-Juárez, N., Arenas, I., Gómez, I., Sánchez-López, R., Arroyo, R., Holzenburg, A., Savva, C. G., Soberón, M., and Bravo, A. (2009) *Biochim. Biophys. Acta* **1788**, 2229-2237.

Nunez-Valdez, M., Sánchez, J., Lina, L., Güereca, L., and Bravo, A. (2001) *Biochim. Biophys. Acta* **1546**, 122-131.

Ounjai, P., Unger, V. M., Sigworth, F. J., and Angsuthanasombat, C. (2007) *Biochem. Biophys. Res. Commun.* **361**, 890-895.

Pardo-López, L., Soberón, M., and Bravo, A. (2013) *FEMS Microbiol. Rev.* **37**, 3-22.

Peyronnet, O., Nieman, B., Ge´ne´reux, F., Vachon, V., Laprade, R., and Schwartz, J. L. (2002) *Biochim. Biophys. Acta* **1567**, 113-122.

Peyronnet, O., Vachon, V., Schwartz, J. L., and Laprade, R. (2001) *J. Membr. Biol.* **184**, 45-54.

Pigott, C. R., and Ellar, D. J. (2007) *Microbiol. Mol. Biol. Rev.* **71**, 255-281.

Pornwiroon, W., Katzenmeier, G., Panyim, S., and Angsuthanasombat, C. (2004) *J. Biochem. Mol. Biol.* **37**, 292-297.

Puntheeranurak, T., Stroh, C., Zhu, R., Angsuthanasombat, C., and Hinterdorfer, P. (2005) *Ultramicroscopy* **105**, 115-124.

Puntheeranurak, T., Uawithya, P., Potvin, L., Angsuthanasombat, C., and Schwartz, J. L. (2004) *Mol. Membr. Biol.* **21**, 67-74.

Regis, L., Silva-Filha, M. H., Nielsen-LeRoux, C., and Charles, J. F. (2001) *Trends Parasitol*. **17**, 377-380.

Schnepf, E., Crickmore, N., Van, Rie, J., Lereclus, D., Baum, J., Feitelson, J., Zeigler, D. R., and Dean, D. H. (1998) *Microbiol. Mol. Biol. Rev.* **62**, 775-806.

Slatin, S. L., Abrams, C. K., and English, L. (1990) *Biochem. Biophys. Res. Commun.* **169**, 765-772.

Sramala, I., Leetachewa, S., Krittanai, C., Katzenmeier, G., Panyim, S., and Angsuthanasombat, C. (2001) *J. Biochem. Mol. Biol. Biophys.* **5**, 219-225.

Tapaneeyakorn, S., Pornwiroon, W., Katzenmeier, G., and Angsuthanasombat, C. (2005) *Biochem. Biophys. Res. Commun.* **330**, 519-525.

Taveecharoenkool, T., Angsuthanasombat, C., and Kanchanawarin, C. (2010) *PMC Biophys.* **3**, 1-16.

Tiewsiri, K., and Angsuthanasombat, C. (2007) *J. Biochem. Mol. Biol.* **40**, 163-171.

Tiewsiri, K., Fischer, W., and Angsuthanasombat, C. (2009) *Arch. Biochem. Biophys.* **482**, 17-24.

Zhan, H., Elliott, J.L., Shen, W.H., Huynh, P.D., Finkelstein, A.,and Collier, R.J. (1999) *J. Membr. Biol.* **167**, 173-181.

Outputs

1. Publications

1.1. Research Articles:

1. Thammasittirong, A., Dechklar, M., Leetachewa, S., Pootanakit, K. & **Angsuthanasombat, C.** (**2011**) *Aedes aegypti* membrane-bound alkaline phosphatase expressed in *Escherichia coli* retains high-affinity binding for *Bacillus thuringiensis* Cry4Ba toxin. ***Appl. Environ. Microbiol.*** 77: 6836-6840. (***5-Year IF*** = ***4.406***)

2. Dechklar, M., Tiewsiri, K., **Angsuthanasombat, C.** & Pootanakit, K. (**2011**) Functional expression in insect cells of glycosylphosphatidylinositol-linked alkaline phosphatase from *Aedes aegypti* midgut larvae: a *Bacillus thuringiensis* Cry4Ba toxin-receptor. ***Insect Biochem. Mol. Biol***. 41: 159-166. (***5-Year IF*** = ***3.620***)

3. Lailak, C., Khaokhiew, T., Promptmas, C., Promdonkoy, B., Pootanakit, K. & **Angsuthanasombat, C**. (**2013**) *Bacillus thuringiensis* Cry4Ba toxin employs two receptor-binding loops synergistic interactions with Cyt2Aa2. ***Biochem. Biophys. Res. Commu.*** 435: 216–221. (***5-Year IF*** = ***2.500***)

4 Juntadech, T., Kanintronkul, Y., Karnchanawarin, C., Katzenmeier, G. & **Angsuthanasombat, C**. (**2013**) Importance of polarity of the α4-α5 loop residue–Asn^{166} in the pore-forming domain of the *Bacillus thuringiensis* Cry4Ba toxin: implications for ion permeation and pore opening. ***J. Biol. Chem.*** (*Under Review*). (***5-Year IF*** = ***5.498***)

4 Imtong, C., Karnchanawarin, C., Katzenmeier, G. & **Angsuthanasombat, C**. (**2013**) Structural importance of the α4-α5 loop within the pore-forming domain of the *Bacillus thuringiensis* Cry4Aa δ-endotoxin. ***Biochim. Biophys, Acta*** (*Under Review*). (***5-Year IF*** = ***3.012***)

1.2. International Meeting Abstracts:

1. **Angsuthanasombat, C.**, Thammasittirong, A., Kanchanawarin, C., Katzenmeir, G., Drechsel, H., Pootanakit, K. Leetachewa, S. & Sakdee, S. (**2012**) Structural insights into insecticidal mechanisms of mosquito-specific toxins from *Bacillus thuringiensis*. In *Abstract of the 6th Pure and Applied Chemistry International Conference 2012-PACCON 2012-Chemistry Beyond Boundaries*, 11-13 January 2012, Chiang Mai, Thailand.

2. Thammasittirong, A., Okahata, Y. & **Angsuthanasombat, C.** (**2012**) High-affinity interactions between *Aedes aegypti* membrane-bound alkaline phosphatase and *Bacillus thuringiensis* Cry4Ba toxin. In *Abstract of the 56th Annual Meeting of the Biophysical Society*, 25-29 February, 2012, San Diego, California, USA.

2. Student Graduated in Ph.D. (*Molecular Genetics and Genetic Engineering*):

1. **Dr. Anon Thammasittirong** (RGJ-10)
2. **Dr. Thanate Juntadech** (RGJ-10)